A Geometric Sufficient Condition for Contact Wrench Feasibility

Shenggao Li[1], Hua Chen[2], Wei Zhang[2], and Patrick M. Wensing[1]

***Abstract*—A fundamental problem in legged locomotion is to verify whether a desired trajectory satisfies all physical constraints, especially those for maintaining contacts. Although foot tipping can be avoided via the Zero Moment Point (ZMP) condition, preventing foot sliding and twisting leads to the more complex Contact Wrench Cone (CWC) constraints. This paper proposes an efficient algorithm to certify the inclusion of a net contact wrench in the CWC on flat ground with uniform friction. In addition to checking the ZMP criterion, the proposed method also verifies whether the linear force and the yaw moment are feasible. The key step in the algorithm is a novel exact geometric characterization of the yaw moment limits in the case when the support polygon is approximated by a single supporting line. We propose two approaches to select this approximating line, providing an accurate inner approximation of the ground truth yaw moment limits with only 18.80% (resp. 7.13%) error. The methods require only $1/150$ (resp. $1/139$) computation time compared to the exact CWC based on conic programming. As a benchmark, approximating the CWC using square friction pyramids requires similar computation time as the exact CWC, but has $> 19.35\%$ error. Unlike the ZMP condition, our method provides a sufficient condition for contact wrench feasibility.**

***Index Terms*—Body Balancing, Humanoid and Bipedal Locomotion, Whole-Body Motion Planning and Control**

I. Introduction

FOR many legged robots, managing contacts with the environment is the key to locomotion. Dynamics constraints related to contact preservation thus present a physical feasibility condition for motion (which may be described as stability conditions in some contexts [1]–[4]). Determining the feasibility of the desired motion is critical since once the desired net contact wrench violates contact constraints, the robot will slide or tip over, potentially leading to a fall, when attempting the motion. Even though unexpected yaw sliding was not always considered as a loss of balance [1], practical experiments and analysis on robots [5] and humans [6] indicate the importance of considering the yaw moment limitations during legged locomotion, including in cases where foot rotation is intended [7].

Manuscript received: June, 30, 2022; Revised Sept, 25, 2022; Accepted Oct, 17, 2022.

This paper was recommended for publication by Editor Abderrahmane Kheddar upon evaluation of the Associate Editor and Reviewers' comments.

This work was supported in part by NSF grant CMMI-2220924, by National Natural Science Foundation of China under Grant No. 62073159 and 62003155.

[1]University of Notre Dame, South Bend, IN, US. {sli25,pwensing}@nd.edu

[2]Southern University of Science and Technology, Shenzhen, China. {chenh6,zhangw3}@sustech.edu.cn

Corresponding author: Shenggao Li

Digital Object Identifier (DOI): see top of this page.

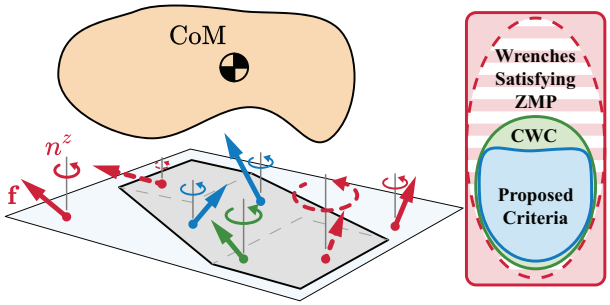

Fig. 1. Net contact wrenches at associated ZMP positions for a robot on a flat ground. Red arrows represent the infeasible wrenches but the dashed ones satisfy the ZMP condition. Green and blue arrows represent feasible wrenches and the blue ones satisfy the proposed feasibility condition. The diagram demonstrates the inclusion relationship within different criteria. The red region contains infeasible wrenches, with the striped area representing wrenches that satisfy the ZMP condition. The inclusion implies that the proposed conditions are sufficient but not necessary for contact wrench feasibility.

A. Related Work

The Zero-Moment-Point (ZMP) condition [8], [9] (i.e., requiring the ZMP to be inside the support polygon) is one of the most widely used feasibility criteria from bipedal robot walking to human biomechanics studies. Since its introduction in 1968, many researchers have extended the ZMP for complex contact scenarios. For example, Harada *et al.* studied the ZMP condition with multi-contacts involving hands [10], Hirukawa *et al.* introduced a generalized ZMP with non-coplanar contacts [3] and then developed a walking pattern generator on uneven terrains [11]. All the above work assumed that surface friction is adequate, such that its limitations can be ignored. As a result, one can show that the ZMP condition is a necessary but not sufficient condition of contact feasibility [2], [3], i.e., the foot can still slide or rotate tangentially on the ground even when the ZMP condition is satisfied, as depicted in Fig. 1.

Some researchers have treated wrench feasibility with friction limitation by restricting the yaw moment to zero: Bretl and Lall computed the static equilibrium support region over uneven terrains [12], and Caron *et al.* constructed the 3D volume of Center of Mass (CoM) accelerations with multi-contacts [13]. The limitation of the ZMP condition sometimes also requires the robot to move its upper body to compensate for the yaw movement of the lower body. Such yaw compensation behaviors have been studied for actuated robot control [5], [14], [15], passive walker design [16], and in human biomechanics [6].

To address the limitations of the ZMP and its generalizations, the exact Contact Wrench Cone (CWC) can be considered [17]. For most legged robots (especially humanoids), due to the full/over actuation condition of the contact surface,

verifying that a net contact wrench lies within the CWC often leads to a force distribution problem (FDP), which can be formulated as a second-order cone program [18], [19]. Even though such a problem can be solved rapidly ($\leq 1ms$ in our testing cases), some applications like real-time simulation or dynamics filtering [20] may benefit from a faster approach.

One widely implemented simplification is to consider polyhedral friction cones and an associated polyhedral approximation of the CWC [21]–[23] in either its span or face form. While construction of the span form is direct, checking for wrench feasibility with it requires similar computation time as with the exact CWC. Conversion from span to face form enables more rapid checking of the CWC condition, but requires a one-time cost for converting between representations (e.g., using double description algorithms [24]). This approach enables Audren *et al.* [19] and Caron *et al.* [4] to plan CoM motions without having to explicitly optimize over all contact forces. One step further, Orsolino *et al.* [25] combined the linearized friction cone with the actuation feasibility polytope to take actuation limitations into account. Although the double description only needs to be computed at every touchdown and lift-off event, it is still computationally expensive ($2.4ms$ for a humanoid robot in [13]), and in practice, the robot may still need to solve an FDP to ultimately determine the actuations for each limb.

For the special case of a rectangular support polygon with aligned friction pyramids, the CWC admits an explicit analytical representation [2]. Notably, this representation can be used to provide analytical limits on the yaw moments as a function of the ZMP position and contact force. However, efficient and accurate feasibility limits on the yaw moment have not been developed under broader situations. As a result, in practice, people often approximate the upper/lower bound on the yaw moment as a linear function of the normal force [26], [27] and norm of tangential force [20]. The yaw moment limitations, however, are also highly related to the direction of force, the position of ZMP, and shape of the support polygon. The lack of treatment for the yaw moment limits within the ZMP criteria motivates this study to find an efficient and accurate strategy for verifying the feasibility of a given net contact wrench on flat ground.

B. Contribution

This paper presents a framework to find an inner approximation of the CWC on rigid flat ground. The contributions of this study are as follows: first, we demonstrate that considering a single supporting line to replace the entire support polygon leads to a faithful approximation of wrench feasibility for most practical support polygons. Second, as the primary contribution, we detail a geometric solution to an optimal FDP on a line segment for characterizing yaw moment limits at the ZMP. It provides an exact solution when the support polygon is a line (e.g., during a quadruped trotting). Third, we propose two approaches with different speed-accuracy tradeoffs to approximate the best choice of the supporting line. As a result, the proposed approaches 1 (resp. 2) experience only 18.80% (resp. 7.13%) error with roughly 150 (resp. 139) times faster computation speed compared to solving the CWC feasibility problem. As a benchmark, the widely used polyhedral approximation with square pyramidal friction cones requires similar computation time as the exact CWC but has $> 19.35\%$ error. The source of the error has been carefully analyzed to provide a deep understanding of both proposed approaches.

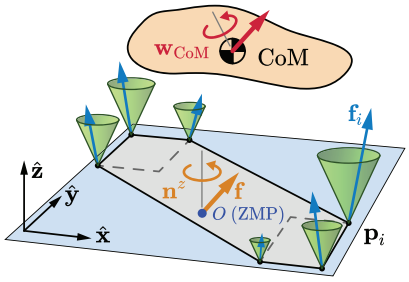

Fig. 2. The illustration of the wrench feasibility problem on flat ground.

II. Background & Problem Formulation

Consider a robot moving in the environment by interacting with the ground through a supporting area modeled by a convex polygon with N vertices $\mathcal{P} = \text{Conv}(\{\mathbf{p}_i \mid i = 1, \dots, N\})$ as in Fig. 2. Suppose the ground is flat with uniform friction coefficient μ and denote the net contact wrench at the CoM by $\mathbf{w}_{\text{CoM}}$. Verifying the feasibility of a net wrench often leads to a FDP, where the linear force $\mathbf{f}_i = [\mathbf{f}_i^{t\top} \ f_i^z]^\top$ applied at the i-th vertex must satisfy the friction cone constraint $\mathbf{f}_i \in \mathcal{C} := \{\mathbf{f} \mid \|\mathbf{f}^t\| \leq \mu f^z\}$ as shown in Fig. 2, where $\mathbf{f}^t$ and f^z denote the tangential (x-y plane) and the normal (z-axis) components, respectively.

A. Contact Wrench Cone Problem

A general approach to verify whether a given net wrench is feasible is to solve the following feasibility problem

$$\text{find} \ \ \mathbf{f}_1, \dots, \mathbf{f}_N \tag{1a}$$

$$\text{s.t.} \ \sum_i^N {}^{\text{CoM}}\mathbf{X}_i^* \begin{bmatrix} \mathbf{0}_{3\times 1} \\ \mathbf{f}_i \end{bmatrix} = \mathbf{w}_{\text{CoM}} \tag{1b}$$

$$\mathbf{f}_i \in \mathcal{C} \tag{1c}$$

where $\mathbf{0}_{3\times 1} \in \mathbb{R}^3$ is a zero vector, $\mathbf{w}_{\text{CoM}} \in \mathbb{R}^6$ is the net contact wrench, and the ${}^{\text{CoM}}\mathbf{X}_i^*$ gives the spatial force transformation matrix [28] from vertex $\mathbf{p}_i$ to the CoM.

This problem is a second-order cone problem (SOCP), and is called the Contact Wrench Cone (CWC) problem. The conic constraint (1c) is often approximated by friction pyramids via $\overline{\mathcal{C}} := \{\mathbf{f} \mid \mathbf{A}\mathbf{f} \leq \mathbf{b}\}$, resulting in a Linear Program. For clarity, we call the feasible set of wrenches for (1) the second-order CWC (2^{nd}-CWC), with the corresponding pyramid approximation as the first-order CWC (1^{st}-CWC).

While we treat the CWC as representing ground truth feasible wrenches (similar to other works [2]–[4], [21]), we openly acknowledge some of its limitations. The vertex force formulation (1) gives the same feasible wrenches as those from an arbitrary friction-satisfying pressure distribution [2].

However, nature does not allow arbitrary pressure distributions. Discontinuous pressure distributions (e.g., with pressure concentrated at vertices) are approximations of what could be provided by true compliant surfaces, and these considerations are not addressed by the CWC. Please see [29], [30] for other perspectives that address such limitations.

B. Zero Moment Point Criterion

Well before the advent of broadly available convex optimization tools, Vukobratovic *et al.* developed the Zero Moment Point (ZMP) criteria to check wrench feasibility for flat ground [8], [9]. The ZMP is noted as O and is defined as the unique point on the ground such that the net wrench at O has only linear force $\mathbf{f}$ and yaw moment n^z (i.e., O satisfies the constraint ${}^O\mathbf{X}^*_{\mathrm{CoM}}\mathbf{w}_{\mathrm{CoM}} = [n^z\hat{\mathbf{z}}^\top \ \mathbf{f}^\top]^\top$ for some n^z and $\mathbf{f}$, where $\hat{\mathbf{z}}$ denotes the unit vector along the z-axis). Note that for readability, all force and moment vectors without subscript are considered at the ZMP O. The ZMP position can be obtained via $\mathbf{w}_{\mathrm{CoM}}$ and the CoM position $\mathbf{p}_{\mathrm{CoM}}$ as

$$\mathbf{p}_O(\mathbf{w}_{\mathrm{CoM}}) = \begin{bmatrix} p^x_{\mathrm{CoM}} - \frac{n^y_{\mathrm{CoM}} + p^z_{\mathrm{CoM}} f^y_{\mathrm{CoM}}}{f^z_{\mathrm{CoM}}} \\ p^y_{\mathrm{CoM}} + \frac{n^x_{\mathrm{CoM}} + p^z_{\mathrm{CoM}} f^x_{\mathrm{CoM}}}{f^z_{\mathrm{CoM}}} \\ 0 \end{bmatrix}. \tag{2}$$

The ZMP feasibility condition of the desired net contact wrench $\mathbf{w}_{\mathrm{CoM}}$ is then given by the constraint

$$\mathbf{p}_O(\mathbf{w}_{\mathrm{CoM}}) \in \mathcal{P} \tag{3}$$

Despite its success, the ZMP constraint (3) only provides a necessary condition for wrench feasibility: friction limits are not considered. As a result, even if the ZMP is inside the support polygon, the robot's foot can still slide translationally on the ground or rotationally about the yaw axis. To construct a sufficient criterion, extra conditions are needed to address the gap between the ZMP and CWC.

C. Wrench Feasibility via Constraints Beyond the ZMP

Consider flat ground with uniform friction and a desired net force at a feasible ZMP. In this case, there exist friction-satisfying forces at the vertices (all $\mathbf{f}_i \in \mathcal{C}$) that generate the net force and ZMP if and only if the net force is in the friction cone ($\mathbf{f} \in \mathcal{C}$) [2, Prop. 1]. This condition can be considered as the condition for the foot not to slide translationally. For this fixed force and ZMP position, an upper ($\overline{n}^*$) and a lower bound ($\underline{n}^*$) exist for the feasible net yaw moment as well. Once these limits are obtained from a given net force at a certain ZMP and support polygon, rotational sliding can be prevented by ensuring that the desired yaw moment n^z lies in the interval $[\underline{n}^*, \overline{n}^*]$. Therefore, we can enforce the CWC condition equivalently via three simpler conditions.

Proposition 1. Consider a support polygon $\mathcal{P}$ on flat ground with uniform friction coefficient μ. A desired net contact wrench $\mathbf{w}_{\mathrm{CoM}}$ is feasible if and only if

1) *No tipping*: The associated ZMP satisfies condition (3).
2) *No sliding*: The linear force $\mathbf{f}$ at the ZMP satisfies the friction constraint: $\mathbf{f} \in \mathcal{C}$.
3) *No rotating*: The yaw moment n^z at ZMP is in the feasible range $[\underline{n}^*, \overline{n}^*]$ for the given ZMP and force $\mathbf{f}$.

The interval $[\underline{n}^*, \overline{n}^*]$ exists only if the first two conditions are satisfied. Since the first two conditions can be easily verified, the remaining question is how to obtain $\underline{n}^*$ and $\overline{n}^*$. We note that this proposition is a natural generalization of [2, Prop. 2] to the case of a general support polygon.

Ref. [2] gives closed-form expressions for $\underline{n}^*$ and $\overline{n}^*$ in the special case of rectangular support with friction pyramids. To address more general cases, we consider the following pair of optimization problems

$$\overline{n}^*/\underline{n}^*(\mathbf{f}) = \max_{\mathbf{f}_1,\dots,\mathbf{f}_N, n^z}/\min\, n^z \tag{4a}$$

$$\text{s.t.} \sum_{i=1}^{N} \mathbf{p}_i \times \mathbf{f}_i = n^z\hat{\mathbf{z}} \tag{4b}$$

$$\sum_{i=1}^{N} \mathbf{f}_i = \mathbf{f}, \mathbf{f}_i \in \mathcal{C} \tag{4c}$$

where the differences from (1) are the cost function (4a) and the added optimization variable n^z. Overall, (4) remains an SOCP similar to before. We focus herein on developing a more efficient method to find an inner approximation (denoted as $[\underline{n}, \overline{n}]$) of the ground truth interval.

In what follows, we focus on the maximization (upper bound) to simplify the exposition, as the minimization (lower bound) can be done in a similar way. For the same purpose, without loss of generality, we will set our coordinate system origin at the ZMP O for simplicity.

III. Proposed Geometric Approach

The most challenging part of the CWC problem is the relatively high computational cost with multiple vertices. Meanwhile, a problem with only a single supporting line (namely $\overleftrightarrow{AB}$) can be used to generate an inner approximation to the moment limits via solving

$$V(\mathbf{p}_a, \mathbf{p}_b, \mathbf{f}) = \max_{\mathbf{f}_a, \mathbf{f}_b, n^z} \ n^z \tag{5a}$$

$$\text{s.t. } \mathbf{p}_a \times \mathbf{f}_a + \mathbf{p}_b \times \mathbf{f}_b = n^z\hat{\mathbf{z}} \tag{5b}$$

$$\mathbf{f}_a + \mathbf{f}_b = \mathbf{f}, \mathbf{f}_{a/b} \in \mathcal{C} \tag{5c}$$

where $\mathbf{f}_a$ ($\mathbf{f}_b$) and $\mathbf{p}_a$ ($\mathbf{p}_b$) denote the linear force and the position vector $\overrightarrow{OA}$ ($\overrightarrow{OB}$) for point A (B), respectively. Note that we shall only consider lines that pass through the ZMP point, which is implicitly embedded in the constraint (5b).

Since we still have the freedom in choosing the location of points A and B, we can further maximize n^z over all possible supporting lines

$$\overline{n}_{\mathrm{line}}(\mathbf{f}) = \max_{\mathbf{p}_a, \mathbf{p}_b} \ V(\mathbf{p}_a, \mathbf{p}_b, \mathbf{f}) \tag{6a}$$

$$\text{s.t. } \mathbf{p}_{a/b} \in \mathcal{P} \tag{6b}$$

Note that, at least one pair of points A and B on the polygon edge is an optimal choice since any line segment $\overleftrightarrow{AB}$ can be extended to touch two edges, and such extensions only increase the feasible moments for the line. Thus, we can replace (6b) with a boundary constraint $\mathbf{p}_{a/b} \in \partial\mathcal{P}$, where

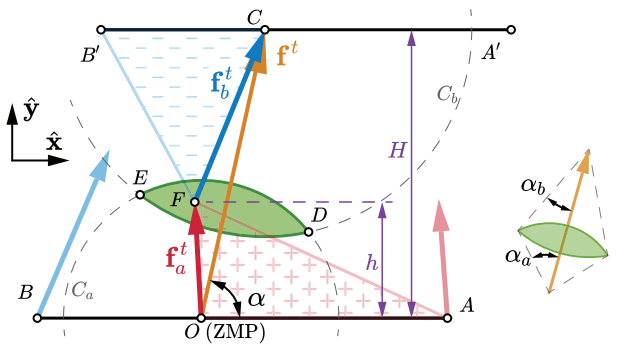

Fig. 3. Geometric structure for solving the optimal force distribution problem on a line. The feasible region (green) for point F (representing $\mathbf{f}_a^t$) is constrained by circles C_a and C_b. Filling with plus signs (resp. minus signs) represents positive (resp. negative) yaw moment contributions.

$\partial\mathcal{P}$ is the boundary of the support polygon. Section III-A first gives an exact solution to (5), and Section III-B then builds upon this solution to approximately solve (6).

A. Solving (5): Force Distribution on a Supporting Line

This section solves (5) via a geometric construction that determines the exact max yaw moment for a given constant net force and a given supporting line with a fixed ZMP on it. We again consider the endpoints A and B, and without loss of generality, assume that ray $\overrightarrow{BA}$ is aligned with the x-axis. We proceed to optimize the forces $\mathbf{f}_a$ and $\mathbf{f}_b$ at these endpoints.

Since the tangential moment at the ZMP must be zero, we can formulate the following equality

$$\|\mathbf{p}_a^t\| f_a^z - \|\mathbf{p}_b^t\| f_b^z = 0 \tag{7}$$

where $\mathbf{p}_a^t = \overrightarrow{OA}$, $\mathbf{p}_b^t = \overrightarrow{OB}$ are the tangential position vectors of the points A and B, respectively. Substituting this equation to the last row of constraint (5c) gives the following relation:

$$f_{a/b}^z = f^z \frac{\|\mathbf{p}_{b/a}^t\|}{\|\mathbf{p}_a^t\| + \|\mathbf{p}_b^t\|} \tag{8}$$

Consequently, we can simplify (5) into a quadratically constrained linear program posed only over the tangential portion of the forces as

$$V(\mathbf{p}_a, \mathbf{p}_b, \mathbf{f}) = \max_{\mathbf{f}_a^t, \mathbf{f}_b^t} \mathbf{p}_a^t \times \mathbf{f}_a^t + \mathbf{p}_b^t \times \mathbf{f}_b^t \tag{9a}$$

$$\text{s.t. } \mathbf{f}_a^t + \mathbf{f}_b^t = \mathbf{f}^t,\ \|\mathbf{f}_{a/b}^t\| \le \mu f_{a/b}^z. \tag{9b}$$

We proceed to solve this simplified problem geometrically.

We start by representing (9b) geometrically. As shown in Fig. 3, we draw the net tangential force $\mathbf{f}^t$ as $\overrightarrow{OC}$ at the application ZMP O and duplicate the supporting line $\overleftrightarrow{AOB}$ to $\overleftrightarrow{A'CB'}$ for convenience. Since $\mathbf{f}_a^t + \mathbf{f}_b^t = \mathbf{f}^t$, we can draw the vector $\mathbf{f}_a^t$ as $\overrightarrow{OF}$ and vector $\mathbf{f}_b^t$ as $\overrightarrow{FC}$. Due to the friction limit (9b), point F must lie within the circle C_a of radius μf_a^z at point O. Similarly, point F must be within the circle C_b with radius μf_b^z at point C as well. Combining the above together, we now have the constraint for the point F as $F \in C_a \cap C_b$. As shown in Fig. 3, the green region $C_a \cap C_b$ is bounded by two arcs $\overset{\frown}{DE}$ (upper side) and $\overset{\frown}{ED}$ (lower side)[1].

[1]Note: we distinguish arcs by notating them in counterclockwise order and define the point right to the tangential force as D.

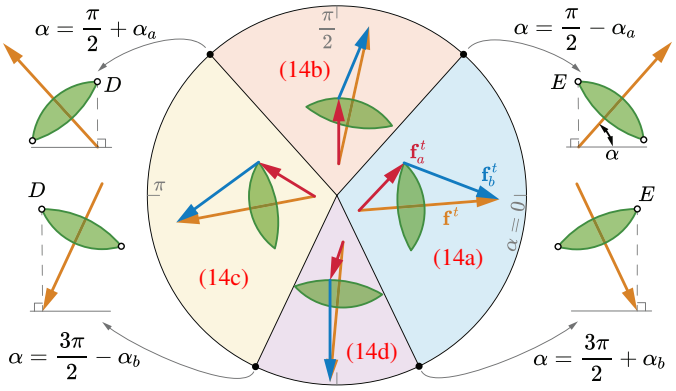

Fig. 4. Four cases for the maximum yaw moment function (14). The cases depict how the optimal vertex forces (blue and red) change as the total horizontal force $\mathbf{f}^t$ (orange) rotates with angle α (shown in Fig. 3). As α changes, the supporting line ($\overleftrightarrow{AOB}$ in Fig. 3) stays fixed, while the construction line ($\overleftrightarrow{B'CA'}$ in Fig. 3) translates with the endpoint of $\mathbf{f}^t$.

With the constraints characterized, we proceed to give a geometric interpretation of the objective (9a). The moment created by $\mathbf{f}_a^t$ takes the cross product between the force vector and the position vector. In geometry, the absolute value of the cross product represents the area of the parallelogram that the vectors span. Such an area is twice the red triangle $\triangle OAF$. Similarly, we can draw the blue triangle $\triangle CB'F$ to represent the moment caused by $\mathbf{f}_b^t$. In Fig. 3, a triangle filled with plus (minus) signs represents a positive (negative) yaw moment contribution. We introduce two variables for readability, $H = f^y$ for the height of point C and $h = f_a^y$ for the height of point F, and reformulate the yaw moment (9a) as

$$n^z = \|\mathbf{p}_a\| h + \|\mathbf{p}_b\| (h - H) \tag{10}$$

Therefore maximizing the yaw moment is equivalent to maximizing the variable h, i.e.,

$$\max_h \underbrace{(\|\mathbf{p}_a\| + \|\mathbf{p}_b\|)}_{\text{given constant}} h - \underbrace{\|\mathbf{p}_b\| H}_{\text{given constant}} \tag{11}$$

The implication is then that, for line $\overleftrightarrow{AB}$ in a horizontal orientation, the yaw moment is maximized when point F is placed at the "highest" point in the green region.

To find this highest point explicitly, we consider how the angle of the force $\mathbf{f}^t$ will influence the orientation of the green region $C_a \cap C_b$. Let us denote the angle $\angle COE$ as α_a and $\angle OCD$ as α_b and define the angle between ZMP force $\mathbf{f}^t$ and the line OA as α (Fig. 3). We can compute α, α_a, and α_b via

$$\alpha = \operatorname{atan2}(f^y, f^x) \tag{12}$$

$$\alpha_{a/b} = \arccos\left(\frac{\|\mathbf{f}^t\|^2 + (\mu f_{a/b}^z)^2 - (\mu f_{b/a}^z)^2}{2\mu f_{a/b}^z \|\mathbf{f}^t\|}\right) \tag{13}$$

The geometric structure shows that there are four different scenarios for the maximum when $C_a \cap C_b$ is a combination of two arcs, as in Fig. 4:

$$\mathbf{f}_a^t = \begin{cases} \mathbf{p}_e^t & \alpha \in (\frac{3\pi}{2} + \alpha_b, \frac{\pi}{2} - \alpha_a] \quad (14a) \\ \mu f_a^z \mathbf{p}_a^\perp & \alpha \in (\frac{\pi}{2} - \alpha_a, \frac{\pi}{2} + \alpha_a] \quad (14b) \\ \mathbf{p}_d^t & \alpha \in (\frac{\pi}{2} + \alpha_a, \frac{3\pi}{2} - \alpha_b] \quad (14c) \\ \mathbf{f}^t + \mu f_b^z \mathbf{p}_a^\perp & \alpha \in (\frac{3\pi}{2} - \alpha_b, \frac{3\pi}{2} + \alpha_b] \quad (14d) \end{cases}$$

Algorithm 1 Max Yaw Moment

Input: $\mathbf{p}_a^t, \mathbf{p}_b^t, \mathbf{f}^t, f^z$

1: $\alpha \leftarrow$ (12), $\alpha_{a/b} \leftarrow$ (13)
2: Compute $\mathbf{p}_e^t$ and $\mathbf{p}_d^t$
3: $\mathbf{f}_a^t \leftarrow$ (14)
4: $\mathbf{f}_b^t = \mathbf{f}^t - \mathbf{f}_a^t$
5: $\overline{n} \leftarrow \mathbf{p}_a^t \times \mathbf{f}_a^t + \mathbf{p}_b^t \times \mathbf{f}_b^t$

Output: $\overline{n}$

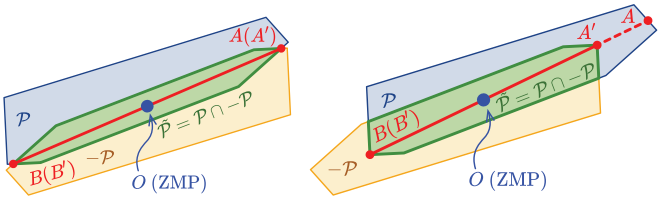

(a) (b)

Fig. 5. The illustration of approach 1: find the longest centered line. The blue and orange polygons give the original support polygon $\mathcal{P}$ and its centro-symmetric $-\mathcal{P}$. The green region is the intersection of $\mathcal{P}$ and $-\mathcal{P}$. The red solid line represents the longest line inside the green region. (a) The intersection of boundaries forms the longest line. (b) The original vertex forms the longest centered line, extension needed. Line AB is the selected support line.

where $\mathbf{p}_a^\perp$ is the normalized vector perpendicular to $\overleftrightarrow{AB}$ and pointing up. Please see the supplementary video for a visual explanation. Transitions between cases occur when points D or E are directly above O or directly below C (Fig. 4). Also, note that there are some special cases when $C_a \cap C_b$ is not two arcs but a single point or an entire circle. In those special cases, the four scenarios would degenerate into one.

Above all, we find a purely geometric solution for the FDP on a supporting line (5). The analytical solution is summarized by the pseudocode in Alg. 1. Returning to the big picture (Prop. 1), we emphasize that this algorithm and its resulting moment limits depend on the linear force $\mathbf{f}$.

B. Line Selection

Since the optimal solution $\overline{n}_{\text{line}}(\mathbf{f})$ of (6) is particularly hard to compute, an alternative way to find a sub-optimal value $\overline{n}(\mathbf{f})$ is needed. Two approaches are considered.

1) Line Selection Approach 1: ***Longest Centered Line****:* One heuristic insight is that a longer supporting line generally enables creating a larger yaw moment, due to the increased moment arm length. In practice, we found the following strategy works reasonably well: finding the longest centered line $\overleftrightarrow{A'OB'}$ (namely $\|B'O\| = \|OA'\|$) crossing the ZMP inside the polygon, then extending it to the original boundary.

To construct such a line, we find the intersection $\tilde{\mathcal{P}}$ of the original polygon $\mathcal{P}$ and its symmetric polygon $-\mathcal{P}$ about the ZMP O. We then enumerate all vertices of $\tilde{\mathcal{P}}$ to find the point $\tilde{P}_j$ furthest from the ZMP. We then extend the line $\overleftrightarrow{O\tilde{P}_j}$ back to the support polygon $\mathcal{P}$ if necessary (as in Fig. 5(b)) since extensions only increase the feasible moments for a line. This procedure is summarized in Alg. 2.

2) Line Selection Approach 2: ***Vertex Enumeration****:* Another approach with more accuracy but slightly more computational cost is powered by the incredible speed of explicit solution in Section III-A, and inspired by the same heuristic that the longer supporting lines generally provide an opportunity to provide additional yaw moment.

Algorithm 2 Find the Longest Centered Line

Input: $\mathcal{P}$: support polygon as a convex hull in vertex form $\mathcal{P} = \text{Conv}(\{\mathbf{p}_i \mid i = 1, \ldots, N\})$

1: $-\mathcal{P} = \text{Conv}(\{-\mathbf{p}_i \mid i = 1, \ldots, N\})$
2: $\tilde{\mathcal{P}} \leftarrow \mathcal{P} \cap -\mathcal{P}$
3: $\tilde{P} = \{\tilde{P}_i | i = 1, 2, \ldots, M\} \leftarrow \text{vertices}(\tilde{\mathcal{P}})$
4: $j \leftarrow \arg\max_i \|\tilde{P}_i\|$
5: $\mathbf{p}_a^t, \mathbf{p}_b^t \leftarrow$ intersection between line $\overleftrightarrow{O\tilde{P}_j}$ and $\partial\mathcal{P}$

Output: $\mathbf{p}_a^t$, $\mathbf{p}_b^t$: end points of the chosen supporting line

Proposition 2. The longest segment crossing a ZMP O in a convex polygon $\mathcal{P}$ has at least one endpoint on a vertex.

Proof. Suppose a line segment $\overleftrightarrow{OA}$ where point A is on an edge but not the vertex. The length of this segment is convex in the segment angle θ. We consider another line segment $\overleftrightarrow{OB}$ on the edge that is colinear with $\overleftrightarrow{OA}$ but in the opposite direction. Similarly, the length of $\overleftrightarrow{OB}$ is convex in the segment angle. As a sum of two convex functions, the entire length function of $\overleftrightarrow{AB}$ is convex as well. Therefore, such a line $\overleftrightarrow{AB}$ can have a local minimum length but no local maximum length if both end-points are not on the vertex, i.e., such a situation cannot result in the longest line. □

Therefore, we are only interested in the lines that cross the origin (i.e., ZMP) and a vertex. Rather than finding a sub-optimal line and then computing the yaw moment, we can check the max yaw moment for all such supporting lines, and then pick the one with the maximum result. Due to the efficiency of the analytical solution from the previous subsection, this approach presents as a good candidate, despite requiring more computation than Approach 1.

IV. Result and Analysis

In this section, we use numerical examples to analyze the error source for the proposed approximation approaches. We quantify the accuracy and computation speed over a set of randomly generated test samples to compare the ground truth CWC problem (2^{nd}-CWC), polytopic CWC (1^{st}-CWC) problem with different numbers of edges, and against a baseline grid search for the optimal supporting line in (6). Example code can be located online [31].

A. Testing Samples

For the convenience of the later discussion, we introduce four different support polygons as the test examples (Fig. 6):

1) Typical case with two planar feet (SP-1) Fig. 6(a)
2) Another case with two planar feet (SP-2) Fig. 6(b)
3) Triangle (SP-3) Fig. 6(c)
4) N-gon (15 edges) inscribed in a circle (SP-4) Fig. 6(d)

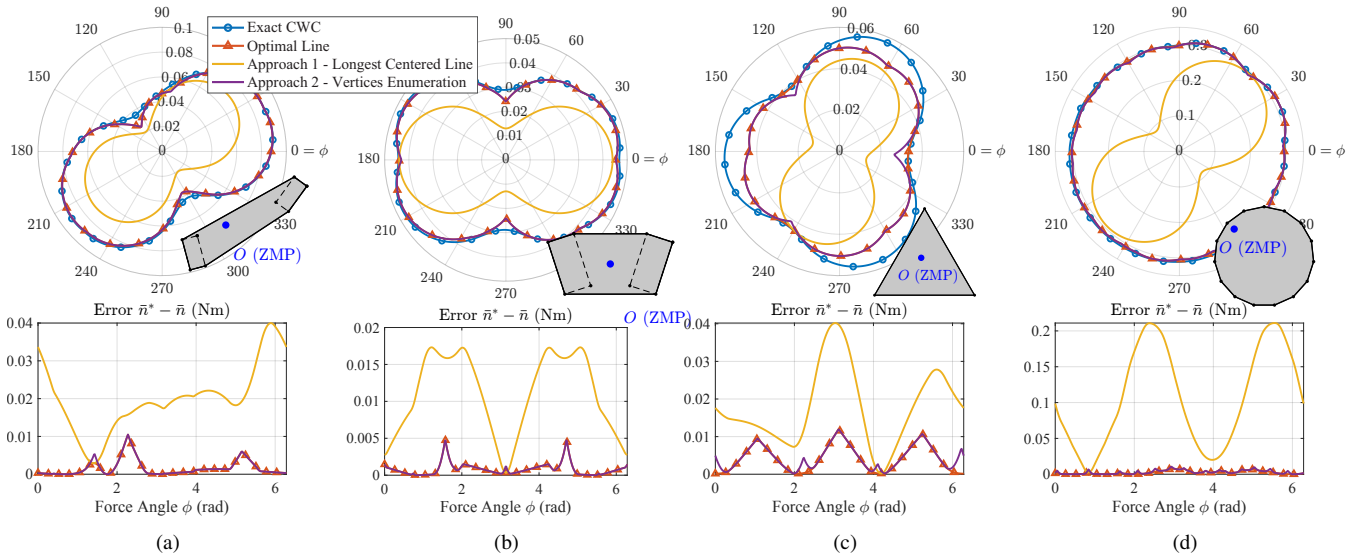

Fig. 6. Comparison between ground truth, optimal line supporting approximation, approach 1, and approach 2 with 4 example cases: (a) SP-1 (see Fig. 7 for additional analysis), (b) SP-2, (c) SP-3, (d) SP-4. The polar plot shows the maximum yaw moment (in Nm) from different algorithms with linear force $\mathbf{f} = [0.84\cos(\phi)\ 0.84\sin(\phi)\ 1]^\top$ N at the ZMP for $\phi \in [0, 2\pi]$ and $\mu = 1$. ZMP positions were randomly chosen within the support polygon.

We test a pure linear force $\mathbf{f}$ applied at a fixed ZMP within the polygon, which is set as the coordinate origin. Note that for any $\mathbf{f}$ and friction coefficient μ, we have

$$\|\mathbf{f}^t\| \leq f^z \mu \iff \left\|\mathbf{f}^t/(f^z\mu)\right\| \leq 1 \tag{15}$$

where $f^z > 0$ and $\mu > 0$, unless the robot is lifting off. Therefore, we can always use a normalized combination $\mathbf{f} = [\mathbf{f}^{t\top}\ 1]^\top$ with $\mu = 1$ to represent all different forces and friction coefficients. Since the max/min yaw moment is highly related to the direction and magnitude of the horizontal force, the tangent force $\mathbf{f}^t$ is parameterized by an angle ϕ in the tangent plane (measure relative to the x-axis) and norm f^t, giving $\mathbf{f}(\phi, f^t) = \begin{bmatrix} f^t\cos(\phi) & f^t\sin(\phi) & 1 \end{bmatrix}^\top$. We present analysis using a horizontal force magnitude of $f^t = 0.84$ at the ZMP positions shown in Fig. 6. The force magnitude of 0.84 is motivated by later analysis in Fig. 7, which shows a relative spike in error at this magnitude.

B. Error Source Analysis

There are two main steps that introduce errors in our strategy. First, we considered restriction to line support situations to approximate the entire support polygon. That means we lose the potential contributions of yaw moments from points off the line (i.e., force distribution on any line will produce less normal moment than force distribution over the full support polygon). Second, none of the heuristic algorithms has a guarantee of finding the optimal line (6), which provides the max/min yaw moment (i.e., the force distribution on the chosen line will produce less normal moments than if the optimal line was chosen).

1) Error from restriction to line support: We evaluate the error introduced by restricting the force distribution to a line by using a dense grid search over line angles (orange triangles in Fig. 6) to find the optimal support line in (6). The gap between this result and the ground truth (blue circles in Fig. 6) gives the theoretical upper bound of any heuristic line finding approach that one could come up with under our framework. It is observed that this approximation works surprisingly well, except when the supporting polygon is a triangle (case (c)). The triangle is the worst case in four examples because all three vertices contribute moments and there is no single line that can accomplish a similar effect. Fig. 6(d) shows that the circle region is an ideal supporting shape for line restriction, which implies that no points off the chosen supporting line offer a significant benefit for generating normal moment.

2) Error from suboptimal line selection: The error caused by heuristically selecting a sub-optimal line leads to the gap between each approach and the optimal line in Fig. 6. Since approach 1 generates new points during the intersection $\mathcal{P} \cap -\mathcal{P}$, it could provide a better result than approach 2 in theory. In practice, the error from approach 2 is smaller in almost all instances, as shown in Fig. 6, second row. The major reason is that the first stage of approach 1 only considers the shape of the support polygon without any information on the linear force, unlike the other. Meanwhile, approach 2 checks the optimal normal moment for all lines crossing the vertices while approach 1 only uses one.

Most importantly, we can find how accurate approach 2 is compared to the theoretical upper bound. Such a result supports the intuition of finding the longest line to approximate the maximum yaw moment. The triangle case becomes the worst case again since there are too few vertices for approach 2 to enumerate. In practice, for polygons with vertices less than a threshold (for example, 4), we can interpolate extra points in-between neighbor vertices to increase the accuracy.

3) Total error vs. force magnitude: The Fig. 7 shows the error of approach 2 compared to the ground truth over different horizontal force magnitudes f^t for the supporting scenario 1 (SP-1, two feet). One can find that the error is consistent across horizontal force magnitudes. As f^t goes to 1, the remaining frictional force at the contact surface goes to 0,

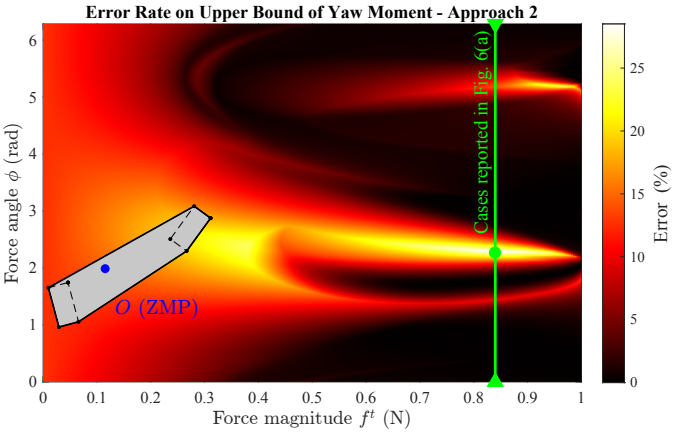

Fig. 7. Error on upper bound ($\overline{n}/\overline{n}^*$) versus magnitude ($\|\mathbf{f}^t\|$) and angle ($\phi$) of horizontal force ($\mathbf{f}^t$) applied at the ZMP. The average error rate is 6.94% with standard deviation 6.20%. The green slice represents the conditions considered in Fig. 6(a). The green dot indicates the peak point.

and the approximation error tends to 0 as well. Such a feature is ideal since the accuracy nearby the contacts' limitation is more critical than others.

C. Quantifying the Performance of Different Approaches

1) Random sample generation: To quantify how accurate and fast the proposed approaches are, we randomly generate test samples with random support polygons and a random force. We quantify the approximation error by computing the fraction of coverage between the approximated yaw moment interval and the ground truth from the CWC as

$$e = 1 - \frac{\overline{n} - \underline{n}}{\overline{n}^* - \underline{n}^*}. \tag{16}$$

In the support polygon sampling part, we randomly pick the points in the rectangular region $\{(-1,-1),(1,1)\}$ to form a polygon (i.e., $p_{i,x},\ p_{i,y} \sim U(-1,1)$). To make the comparison fair and ensure the polygon's convexity, we repetitively pick new points until the convex hull of the given points has 6 vertices (as the most common case in humanoid walking). Then we randomize the polar coordinates of the horizontal force as $\phi \sim U(0,2\pi),\ f^t \sim U(0,1)$.

Table I[2,3] shows the average compute time per sample and accuracy of approaches 1 and 2 compared to the ground truth and all different methods, under 10000 random samples with 6 vertices each. At each point on the horizontal axis of Fig. 8, the cumulative possibility gives the fraction of samples with moment errors (16) below that threshold.

2) Rapid and accurate result of proposed approaches: The most outstanding result in Table I is that while the 2^{nd}-CWC spends $562.28\mu s$ to compute, the two proposed approaches achieve 18.80% (approach 1) or 7.13% (approach 2) relative error within $3.74\mu s$ or $4.04\mu s$. They are ~ 150 or ~ 139 times faster than the ground truth method. While approach 2 is only 11.67% more accurate than approach 1, the

[2]The 1^{st}-CWC and 2^{nd}-CWC were solved on a commodity laptop (2.5 GHz Intel Core i7) by the state-of-the-art interior point solver MOSEK [32] with its C++ API.

[3]The optimal supporting line is solved by a brute force search algorithm with 5000 grid points to ensure accuracy.

TABLE I
PERFORMANCE COMPARISON WITH 6 VERTICES, 10000 SAMPLES

Method	Error	Std. Dev.	Time (μs)
2^{nd}-CWC	0%	0%	562.28
1^{st}-CWC (4 edges)	19.35%	15.02%	676.35
1^{st}-CWC (8 edges)	8.37%	9.94%	951.06
Approach 1	18.80%	16.63%	3.74
Approach 2	7.13%	5.54%	4.04
Grid Search (81 lines)	7.13%	5.56%	51.11
Optimal Supporting Line	6.49%	4.88%	2873.0

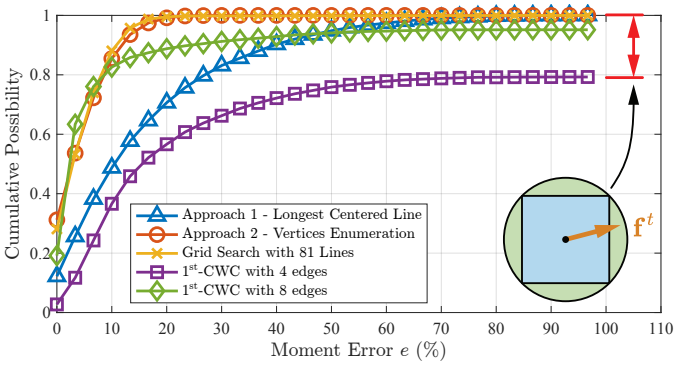

Fig. 8. Cumulative possibility versus moment error (16) for different approaches over 1000 random samples. The 1^{st}-CWC methods do not reach 100% since some feasible forces are outside the friction pyramid.

cumulative possibility plot shows that it more frequently gives a low moment error (16). Therefore, approach 2 is generally more promising with only 8.0% more computation time. It is worth emphasizing that even with a 70% error under some rare ($< 1.4\%$) samples, approach 1 still provides a sufficient condition for feasibility. That means all the error implies the loss of yaw motion ability but not stability.

3) Comparison to the widely used linear CWC: In most of the literature (e.g., [21]–[23]) friction cones are considered as friction pyramids with 4 edges (occasionally 8) to replace the second-order cone constraint with a set of linear constraints. Our result demonstrates that both two proposed approaches are more accurate than the 4 edges 1^{st}-CWC, and approach 2 is even more accurate than the 8 edges version. Note that the 1^{st}-CWC also approximates the feasible region of linear force while the proposed approaches would give an exact region. As a result, there are some (20.65% for 4 edges, 5.14% for 8 edges) feasible testing samples that the 1^{st}-CWC would consider as infeasible as illustrated in Fig. 8. Those samples were removed from the statistical data of 1^{st}-CWC in Table I. Therefore the cumulative possibility of them is never going to 1. The average error reported for the 1^{st}-CWC only considers the remaining samples, and so should be considered as an under approximation of the true error.

Fig. 9 shows the case of a rectangular support polygon, wherein the 1^{st}-CWC admits an analytical solution [2]. Even in this simple case, compared to the average 34.52% error of 1^{st}-CWC, our approach gives a tighter (12.75% error) bound on the true yaw limits due to its consideration of the full friction cone, and despite the approximations of line support considered. Additionally, in Fig. 10, we simulate the worst force magnitude and angle combination for each ZMP in the

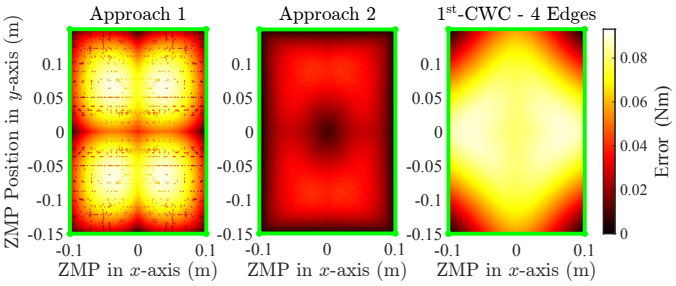

Fig. 9. Approximation error of different approaches versus all feasible choices of ZMP. Green rectangle represents the support polygon. Color at each point represents the average of error $(\overline{n}^* - \underline{n}^*) - (\overline{n} - \underline{n})$ over 1000 randomly chosen forces, as in Section IV-C1.

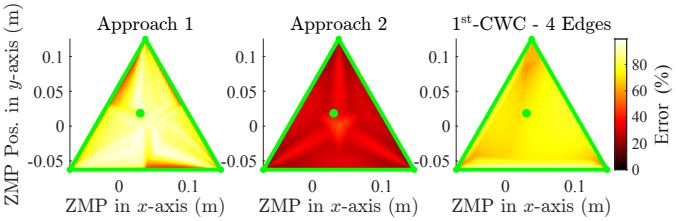

Fig. 10. The maximum moment error (16) heat map for all possible force magnitude and angle combination at each feasible ZMP in the triangle support polygon. The green dot indicates the ZMP considered in Fig. 6(c).

triangle case, the worst scenario considered previously. Even in this situation, our approach 2 still performs strictly better than the 1^{st}-CWC at each ZMP position.

V. Conclusion

This paper presented two geometric approaches to find an inner approximation of the contact wrench cone on flat ground with uniform friction coefficient. The preferred approach 2 can find the sufficient condition of contact wrench feasibility in only $4.04\mu s$ (139 times faster than CWC). It would only sacrifice $< 7.13\%$ on the yaw motion ability. A new geometric construction powered the rapid computation of exact yaw moment limits when the support polygon is a line. This study also provided insights on the error source and the reason of success of proposed approaches. In the future, we are interested in the potential application of this method on a legged robot as a low-level dynamics filter [20] and in rigid-body simulation as a loss of contact criteria.

References

[1] A. Goswami, "Postural stability of biped robots and the foot-rotation indicator (FRI) point," *The International Journal of Robotics Research*, vol. 18, no. 6, pp. 523–533, 1999.

[2] S. Caron, Q.-C. Pham, and Y. Nakamura, "Stability of surface contacts for humanoid robots: Closed-form formulae of the contact wrench cone for rectangular support areas," in *IEEE Int. Conf. on Robotics and Automation*, pp. 5107–5112, 2015.

[3] H. Hirukawa, S. Hattori, K. Harada, S. Kajita, K. Kaneko, F. Kanehiro, K. Fujiwara, and M. Morisawa, "A universal stability criterion of the foot contact of legged robots-adios ZMP," in *IEEE Int. Conf. on Robotics and Automation*, pp. 1976–1983, 2006.

[4] S. Caron, Q.-C. Pham, and Y. Nakamura, "Leveraging cone double description for multi-contact stability of humanoids with applications to statics and dynamics.," in *Robotics: science and systems*, vol. 11, pp. 1–9, 2015.

[5] B. Ugurlu, J. A. Saglia, N. G. Tsagarakis, and D. G. Caldwell, "Yaw moment compensation for bipedal robots via intrinsic angular momentum constraint," *International Journal of Humanoid Robotics*, vol. 9, no. 04, p. 1250033, 2012.

[6] Y. Li, W. Wang, R. H. Crompton, and M. M. Gunther, "Free vertical moments and transverse forces in human walking and their role in relation to arm-swing," *Journal of Experimental Biology*, vol. 204, no. 1, pp. 47–58, 2001.

[7] K. Miura, S. Nakaoka, M. Morisawa, F. Kanehiro, K. Harada, and S. Kajita, "Analysis on a friction based "twirl" for biped robots," in *IEEE Int. Conf. on Robotics and Automation*, pp. 4249–4255, 2010.

[8] M. Vukobratovic and D. Juricic, "Contribution to the synthesis of biped gait," *IEEE Trans. on Biomedical Eng.*, no. 1, pp. 1–6, 1969.

[9] M. Vukobratović and B. Borovac, "Zero-moment point—thirty five years of its life," *International journal of humanoid robotics*, vol. 1, no. 1, pp. 157–173, 2004.

[10] K. Harada, S. Kajita, K. Kaneko, and H. Hirukawa, "ZMP analysis for arm/leg coordination," in *IEEE/RSJ Int. Conf. on Intelligent Robots and Systems*, vol. 1, pp. 75–81, 2003.

[11] H. Hirukawa, S. Hattori, S. Kajita, K. Harada, K. Kaneko, F. Kanehiro, M. Morisawa, and S. Nakaoka, "A pattern generator of humanoid robots walking on a rough terrain," in *IEEE Int. Conf. on Robotics and Automation*, pp. 2181–2187, 2007.

[12] T. Bretl and S. Lall, "Testing static equilibrium for legged robots," *IEEE Trans. on Robotics*, vol. 24, no. 4, pp. 794–807, 2008.

[13] S. Caron and A. Kheddar, "Multi-contact walking pattern generation based on model preview control of 3D COM accelerations," in *IEEE-RAS Int. Conf. on Humanoid Robots*, pp. 550–557, 2016.

[14] P. M. Wensing and D. E. Orin, "Improved computation of the humanoid centroidal dynamics and application for whole-body control," *International Journal of Humanoid Robotics*, vol. 13, no. 01, p. 1550039, 2016.

[15] R. Cisneros, K. Yokoi, and E. Yoshida, "Yaw moment compensation by using full body motion," in *IEEE Int. Conf. on Mechatronics and Automation*, pp. 119–125, 2014.

[16] S. H. Collins, M. Wisse, and A. Ruina, "A three-dimensional passive-dynamic walking robot with two legs and knees," *The International Journal of Robotics Research*, vol. 20, no. 7, pp. 607–615, 2001.

[17] D. J. Balkcom and J. C. Trinkle, "Computing wrench cones for planar rigid body contact tasks," *The International Journal of Robotics Research*, vol. 21, no. 12, pp. 1053–1066, 2002.

[18] P. M. Wensing, G. Bin Hammam, B. Dariush, and D. E. Orin, "Optimizing foot centers of pressure through force distribution in a humanoid robot," *International Journal of Humanoid Robotics*, vol. 10, no. 03, p. 1350027, 2013.

[19] H. Audren and A. Kheddar, "3-D robust stability polyhedron in multi-contact," *IEEE Trans. on Robotics*, vol. 34, no. 2, pp. 388–403, 2018.

[20] K. Yamane and Y. Nakamura, "Dynamics filter-concept and implementation of online motion generator for human figures," *IEEE Trans. on Robotics and Automation*, vol. 19, no. 3, pp. 421–432, 2003.

[21] H. Dai, *Robust multi-contact dynamical motion planning using contact wrench set*. PhD thesis, Massachusetts Institute of Technology, 2016.

[22] H. Dai and R. Tedrake, "Planning robust walking motion on uneven terrain via convex optimization," in *IEEE-RAS Int. Conf. on Humanoid Robots*, pp. 579–586, 2016.

[23] A. Del Prete, S. Tonneau, and N. Mansard, "Zero step capturability for legged robots in multicontact," *IEEE Trans. on Robotics*, vol. 34, no. 4, pp. 1021–1034, 2018.

[24] K. Fukuda and A. Prodon, "Double description method revisited," in *Franco-Japanese and Franco-Chinese Conf. on Combinatorics and Computer Science*, pp. 91–111, Springer, 1995.

[25] R. Orsolino, M. Focchi, C. Mastalli, H. Dai, D. G. Caldwell, and C. Semini, "Application of wrench-based feasibility analysis to the online trajectory optimization of legged robots," *IEEE Robotics and Automation Letters*, vol. 3, no. 4, pp. 3363–3370, 2018.

[26] J. Park and O. Khatib, "Contact consistent control framework for humanoid robots," in *IEEE Int. Conf. on Robotics and Automation*, pp. 1963–1969, 2006.

[27] M. Kanazawa, S. Nozawa, Y. Kakiuchi, Y. Kanemoto, M. Kuroda, K. Okada, M. Inaba, and T. Yoshiike, "Robust vertical ladder climbing and transitioning between ladder and catwalk for humanoid robots," in *IEEE/RSJ Int. Conf. on Intelligent Robots and Systems*, pp. 2202–2209, 2015.

[28] R. Featherstone, *Rigid body dynamics algorithms*. Springer, 2014.

[29] R. D. Howe and M. R. Cutkosky, "Practical force-motion models for sliding manipulation," *The International Journal of Robotics Research*, vol. 15, no. 6, pp. 557–572, 1996.

[30] Y. Gonthier, *Contact Dynamics Modelling for Robotic Task Simulation*. PhD thesis, University of Waterloo, 2007.

[31] S. Li, "GCWF - Verifying Contact Wrench Feasibility via Geometrical Approach." https://github.com/ROAM-Lab-ND/GCWF, 9 2022.

[32] M. ApS, *MOSEK Fusion API for C++. Version 9.3.20*, 2022.